In-Time UAV Flight-Trajectory Estimation and Tracking Using Bayesian Filters

Portia Banerjee
SGT Inc., NASA Ames Research Center
Moffett Field, CA 94035
portia.banerjee@nasa.gov

Matteo Corbetta
SGT Inc., NASA Ames Research Center
Moffett Field, CA 94035
matteo.corbetta@nasa.gov

Abstract*—Rapid increase of UAV operation in the next decade in areas of on-demand delivery, medical transportation services, law enforcement, traffic surveillance and several others pose potential risks to the low altitude airspace above densely populated areas. Safety assessment of airspace demands the need for novel UAV traffic management frameworks for regulation and tracking of vehicles. Particularly for low-altitude UAV operations, quality of GPS measurements feeding into the UAV is often compromised by loss of communication link caused by presence of trees or tall buildings in proximity to the UAV flight path. Inaccurate GPS locations may yield to unreliable monitoring and inaccurate prognosis of remaining battery life and other safety metrics which rely on future expected trajectory of the UAV. This work therefore proposes a generalized trajectory monitoring and prediction methodology for autonomous UAVs using in-time GPS measurements. Firstly, a 4D smooth trajectory generation technique from a series of waypoint locations with associated expected times-of-arrival based on B-spline curves is presented. Initial uncertainty in the vehicle's expected cruise velocity is propagated through the trajectory to compute confidence intervals along the entire flight trajectory using error interval propagation approach. Further, the generated planned trajectory is considered as the prior knowledge which is updated during its flight with incoming GPS measurements in order to estimate its current location and corresponding kinematic profiles. The estimation of the vehicle position is defined in a state-space representation such that the position at a future time step is derived from position and velocity at current time step and expected velocity at the future time step. A linear Bayesian filtering algorithm is employed to efficiently refine position estimation from noisy GPS measurements and update the confidence intervals. Further, a dynamic re-planning strategy is implemented to incorporate unexpected detour or delay scenarios. Finally, critical challenges related to uncertainty quantification in trajectory prognosis for autonomous vehicles are identified, and potential solutions are discussed at the end of the paper. The entire monitoring framework is demonstrated on real UAV flight experiments conducted at the NASA Langley Research Center.

TABLE OF CONTENTS

1. INTRODUCTION

Emerging technology surrounding unmanned aerial vehicles (UAVs) has broadened industrial applications which include, but not limited to, on-demand delivery, medical transportation, precision farming, weather monitoring and traffic surveillance. As a result, density of UAV operations in low-altitude airspace is expected to grow tremendously in the upcoming decades, changing the future of aerospace [1], [2]. Owing to the complexity and risk associated with such massive UAV operations, a holistic and in-time safety assessment of the airspace has become a critical area of research. An un-monitored UAV can not only result in economic loss in the event of a crash but also poses threat to lives and property on ground.

Criticality of state awareness and monitoring for commercial manned aircraft has been identified and implemented widely over the past years ensuring high safety associated with them. Designing of Traffic Collision Avoidance System (TCAS) [3] and the Terrain Awareness Warning System (TAWS) [4] have been powerful risk-mitigation technologies. Besides, operational mitigation performed by 'human pilots' and 'air traffic controllers' based on warnings and alerts issued by real-time safety monitoring tools [5], [6], [7] have played critical role in the exemplary safety record in recent years. However, challenges involving safety assessment of small autonomous UAVs are substantially different from manned aircrafts. Firstly, size, weight and cost constraints restrict installation of heavy and expensive on-board computing systems or hardware for large-bandwidth communications with the ground station, thus limiting the ability to perform self-diagnosis and prognosis. Such constraints limit the size and life of batteries that can be carried by these vehicles. Further, according to current FAA standards, most operations involving small UAVs are expected to occur within 400 feet from ground. As a consequence of low altitude, external disturbances such as wind gusts or turbulence may have stronger effects on UAVs than they have been traditionally studied for larger commercial aircrafts, even potentially accelerating discharge rates from their batteries. Besides, wind tunnel effects caused by buildings or other obstacles in urban environment may jeopardize vehicle stability and are even harder to predict.

For ensuring safe operations in the low-altitude airspace and integrating with the general aviation, there is a consensus in between government and industries that UAVs should be equipped with in-time safety and situational aware (SSA) technologies [8]. NASA's Aeronautics Research Mission Directorate describes a strategic plan for investigating and advancing in-time safety assurance capabilities [9] by integrating information from multiple sources. Information may be (1) vehicle specific such as battery state-of-charge, component's health status, (2) third-party sources such as weather, obstacles and terrain information or (3) from UAV Traffic

Management (UTM) on entire airspace status consisting of multiple UAVs and their mission objectives. As a pre-flight check, UAV first needs to connect to a 'licensed' ground control system (GCS) to 'request' its planned flight path or flight region. If the risks associated with the planned flight which includes monitoring as well as forecast information are found acceptable, the GCS approves the 'request' and the UAV is set to fly. However, discrepancies may occur during flight such as component failure, degraded position estimates or external turbulences causing unplanned delay, hovering or deviation from its planned path. Such discrepancies should be estimated and communicated by the monitoring system to the GCS or UTM in-time to avoid detrimental consequences.

With the goal of achieving in-flight monitoring capabilities, this paper presents a study on in-time estimation of 4D trajectories of small UAVs flying in autonomous mode. The work is based on a state-of-the-art B-spline trajectory generation algorithm in which uncertainty is quantified in terms of variations in its planned cruise speed. Further uncertainty in the estimated position is updated using Bayes filtering based on the quality of position measurements available from on-board navigation system. The approach can assist in-time tracking of UAVs particularly under degraded position measurements. Uncertainty in predicted trajectory due to poor quality of GPS measures directly improves computation of other related safety metrics such as future power consumption profile or proximity to obstacles.

2. UAV Health Monitoring Framework

In-time monitoring of UAVs can be achieved via a simulation model of the UAV flight that is executed on the ground station, or in the cloud, with RF communication link with the real UAV in operation. The model parameters are initialized utilizing available pre-flight information and then updated by additional data as the flight progresses. In order to achieve a comprehensive SSA, the data sources should include (a) On-board navigation sensors (Eg: LIDAR, GPS, IMU) (b) On-board diagnostic sensors (Eg: battery power usage monitors, temperature and pressure sensors, vibration sensors) (c) External data sources (Eg: city plan maps, localized wind information, weather forecasts, crowd density maps, terrain maps).

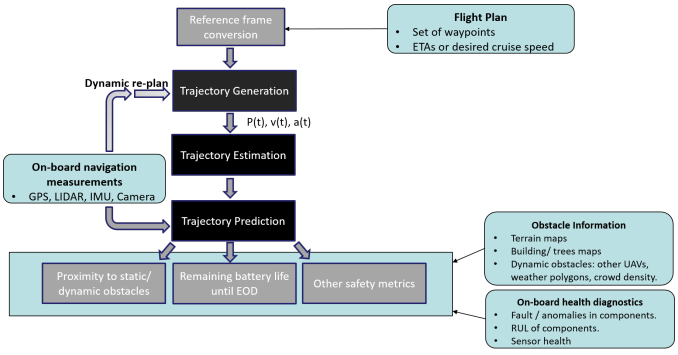

Figure 1. Overall simulation framework: safety monitoring of UAV airspace.

The simulation framework, as depicted in Figure 1, begins with the flight plan or a set of waypoints that the UAV has to traverse through in 4-dimensional coordinates lat, lon, alt, eta where lat, lon, alt represents the geographical location of each waypoint in geodetic coordinate system of latitude ϕ, longitude λ and altitude ζ, with eta representing the expected time-of-arrival at each of them. Before generating and tracking the UAV trajectory, an important step is converting the reference frames of simulation. Although, weather cells and obstacle locations are mostly defined in geodetic frames based on assumption of earth's shape as the WGS84 ellipsoid, proximity of vehicle(s) from obstacle(s) can be easily interpreted within a Cartesian reference frame in terms of linear distances. Hence, a reference frame conversion approach is implemented to convert geodetic coordinates to Cartesian frame which is then sent as an input to the trajectory generation algorithm. In order to convert the geodetic units to a local Cartesian frame, the waypoint positions are first converted to an Earth-Center-Earth Fixed (ECEF) frame according to Eq. (1). In Eq. (4), the values of the equatorial and polar radius of the earth are defined as $a = 6378137$ m and $b = 6356752.314245$ m, respectively.

$$\begin{aligned} X &= (N+\zeta)\cos\phi\cos\lambda \\ Y &= (N+\zeta)\cos\phi\sin\lambda \\ Z &= \big(\zeta + (1-e^2)N\big)\sin\phi \end{aligned} \tag{1}$$

where,

$$N = \frac{a}{\sqrt{1-e^2\sin^2\phi}} \quad , \tag{2}$$

$$e = \sqrt{f(2-f)} \tag{3}$$

$$f = \frac{a-b}{a} \tag{4}$$

Keeping the first waypoint location (X_0, Y_0, Z_0) fixed in the ECEF coordinates, the relative distances of every other waypoint from the first waypoint is then computed according to Eq. (5).

$$\begin{aligned} \Delta X &= X - X_0 \\ \Delta Y &= Y - Y_0 \\ \Delta Z &= Z - Z_0 \end{aligned} \tag{5}$$

Finally, considering the first waypoint as the origin of the local cartesian frame $(0, 0, 0)$, the cooordinates for every other waypoint in the cartesian frame are computed according to (6), where ϕ_0 and λ_0 indicate the latitude and longitude of first waypoint in geodetic frame.

$$\begin{aligned} x &= -\Delta X\sin\lambda_0 + \Delta Y\cos\lambda_0 \\ y &= -\Delta X\cos\lambda_0\sin\phi_0 - \Delta Y\sin\phi_0\sin\lambda_0 + \Delta Z\cos\phi_0 \\ z &= \Delta X\cos\phi_0\cos\lambda_0 + \Delta Y\cos\phi_0\sin\lambda_0 + \Delta Z\sin\phi_0 \end{aligned} \tag{6}$$

Once the waypoint coordinates are obtained in the local ENU frame, the next step in the simulation model is to generate kinematic smooth trajectory traversing through each

waypoint along with the associated confidence bounds. At each time-instant, the expected location of the UAV should be updated with measurements from on-board navigation units, thereby refining prediction of the future trajectory as well as the uncertainty bounds. It is imperative to update planned trajectory with in-time measurements since the subsequent safety metrics such as future power consumption or proximity to dynamic obstacles depend heavily on the accuracy of the predicted trajectory. For example, in the event of off-nominal conditions such as presence of sudden wind gusts or dynamic obstacles, when the UAV deviates from its planned course, safety associated with the remaining trajectory are directly affected including the future power consumption profile or risk to non-participating crowd. The confidence bounds associated with the prediction should also be realistic and based on quality of navigation measurements in order to improve the SSA for a UAV. This paper, therefore, focuses on the trajectory generation, in-time estimation and prediction algorithms based on a pre-defined flight plan and in-time GPS measurements for a UAV, as explained in Section 3 followed by results in Section 4. The same approach can be extended to an airspace consisting of multiple UAVs to compute the overall safety of the UAV airspace.

The following steps of the health monitoring framework includes computation of safety metrics utilizing both on-board health diagnostic information and external data. UAV health diagnostics further include fault identification strategies based on available data sources. Safety metrics may include proximity from static or dynamic obstacles [10], RUL of battery SOC [11] or risk to non-participating crowd [12]. Details of such safety assessment is beyond the scope of this paper. Interested readers are encouraged to follow the relevant literature.

3. UAV TRAJECTORY TRACKING

The trajectory tracking approach proposed in this work grounds on three key elements: (i) a NURBS-based trajectory generation algorithm to estimate the UAV kinematic profile over the entire trajectory, (ii) the quantification of uncertainty affecting the arrival times over the trajectory, and (iii) in-time tracking of the vehicle location through Bayesian filtering of on-board measures and the corresponding kinematic model.

NURBS Trajectory Generation

In order to achieve kinematic smooth trajectories representative of the true, desired trajectory of the vehicle, non-uniform rational B-splines (NURBS) have been implemented in this work. NURBS are parametric composite curves applied in several robotic applications owing to their desirable properties of convex hull and maintaining continuity up to the $k-1$ derivative for a curve of degree k [13], [14], [15]. The final trajectory passes in a convex turn close to every way-point instead of crossing exactly through them, thereby avoiding a complete stop at the way-point locations and maintaining energy-efficiency. Besides, clamped NURBS curves [15] generates a trajectory starting and ending at exact way-point locations, representative of take-off and landing ports.

Given a set of $n+1$ way-points, a NURBS curve is a piecewise curve described by parameter $u \in \mathbb{R}_{\geq 0} : 0 \leq \mathrm{u} \leq \mathrm{n} - \mathrm{k} + 2$, defined according to Eq. (7). This implies that the final curve can be assumed to be composed of $n-k+1$ sections where each section of the curve $\{[0,1],[1,2],...,[(n-k+1),(n-k+2)]\}$ is of degree k. Figure 2 (a) depicts a NURBS curve generated from $n=7$ way-points with desired degree of $k=3$, thereby comprising $7-3+1=5$ sections denoted by $\{C_1, C_2, C_3, C_4, C_5\}$.

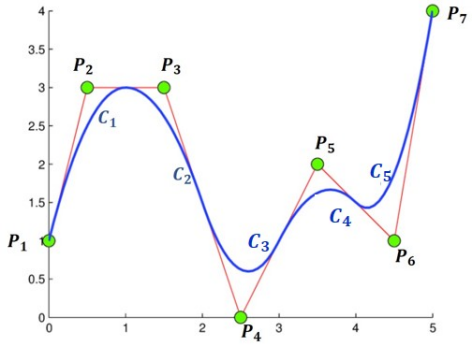

Figure 2. Schematic of NURBS trajectory generation based on example way-points $P_1 - P_7$

Each segment of the NURBS curve is composed by a weighted contribution from each way-point defined according to a basis function $N_{i,k}(u)$ which is computed for i^{th} way-point and k^{th} degree. The NURBS basis function is described in Eqs. (8a) and (8b).

$$x(u) = \frac{\sum_{i=0}^{n} h_i N_{i,k}(u) x_i}{\sum_{i=0}^{n} h_i N_{i,k}(u)}, \quad 0 \leq u \leq n-k+2 \tag{7}$$

$$N_{i,k}(u) = \frac{(u-t_i)N_{i,k-1}(u)}{t_{i+k-1}-t_i} + \frac{(t_{i+k}-u)N_{i+1,k-1}(u)}{t_{i+k}-t_{i+1}} \tag{8a}$$

$$N_{i,1}(u) = \begin{cases} 1 & \text{if } t_i \leq u \leq t_{i+1} \\ 0 & \text{otherwise} \end{cases} \tag{8b}$$

For example, in Figure 2, the degree k was set to 3, hence way-points P_1, P_2, and P_3 defines the curve segment C_1, way-points P_2, P_3 and P_4 defines the curve segment C_2 and and so on for the remaining segments $C_3 - C_5$. Finally, the weight h_i associated with each way-point controls the distance of curve from that way-point. The term t, known as the *knot vector*, is defined in Eq.(9) such that it identifies the way-points that contribute to each segment of the NURBS curve via the basis function.

$$t_i = \begin{cases} 0 & \text{if } i \leq k \\ i-k+1 & \text{if } k \leq i \leq n \\ n-k+2 & \text{if } i \geq n \end{cases} \tag{9}$$

One of the other advantages of using NURBS is that no in-flight parameters are required for generating the trajectory. Both the position and velocity profile of planned trajectory can be obtained using the global locations and expected time of arrival (ETA) at the way-points, which makes this approach applicable for multiple UAVs.

The distance of the resultant curve from each way-point can be controlled by their relative weights. Increasing weights of one way-point ensures that the curve passes close to that way-point but pulls it away from the other way-points. Hence, a

curve passing close to every way-point following sharp turns, similar to a rotor-type UAV flight, could not be achieved by the existing NURBS algorithm. This drawback was solved in one of the previous studies [16] by adding pseudo way-points associated with lower weights in between two consecutive true way-points. The smoothness of the trajectory as well as distance of curve from each way-point could therefore be adjusted by regulating the weights of the true way-points relative to that of the pseudo way-points. Details of the approach are described in [16]. By assigning and varying the weights, the shape of the resultant curve, particularly at the turns, can be adjusted, as shown in Figure 3 (a).

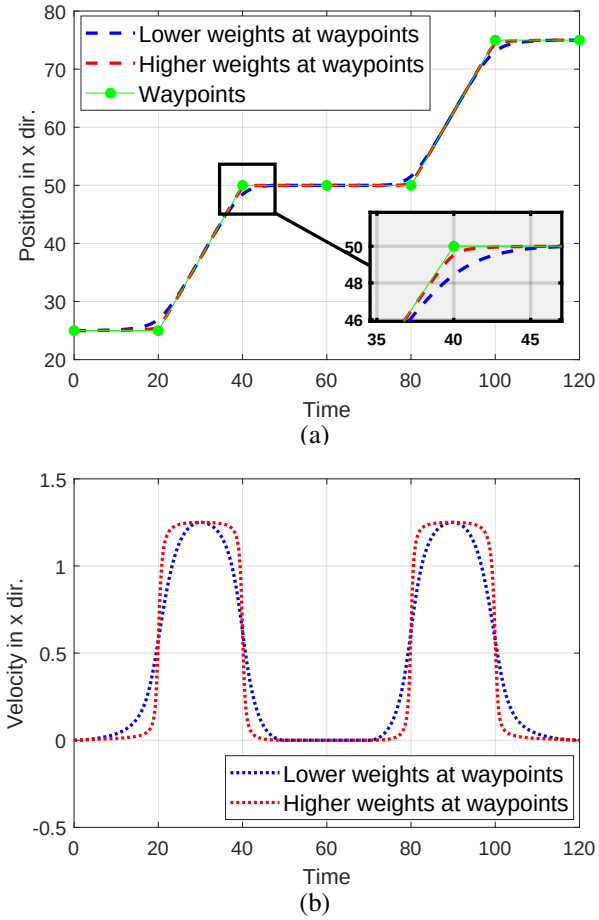

Figure 3. NURBS trajectory from simulated way-points with higher and lower weights of pseudo points (a), and respective velocity profiles (b).

Uncertainty Quantification in Planned Trajectory

The NURBS trajectory generated from a set of way-points is based on a constant velocity profile, exhibiting non-zero accelerations only at the way-points where movement direction changes. However, uncertainty in external variables (e.g., an un-modeled wind field) or performance of the autopilot system may produce delays in the flight execution by causing fluctuations of the vehicle's cruise speed, which eventually lead to different arrival times. This section shows how the uncertainty affecting the times of arrival (TAs) can be estimated by modeling uncertainty in the expected cruise speed. The approach enables the computation of the TA confidence intervals over the entire trajectory profile.

Uncertainty affecting the cruise velocity is modeled using Gaussian independent random variables with covariance $\Sigma_v = I_3 \left[\sigma^2_{v,x}, \sigma^2_{v,y}, \sigma^2_{v,z}\right]^T \in \mathbb{R}^{3\times3}$, where I_3 is a 3×3 identity matrix. The speed profile uncertainty is then propagated through the trajectory using error intervals [17]. The errors affecting the cruise speed along the three directions are assumed to be independent and identically distributed. The outcome is a 4D NURBS trajectory that includes confidence boundaries of the vehicle locations based on the input cruise speed uncertainty. Assuming negligible acceleration, the kinematic relationship between position and time becomes $\Delta t = \Delta p\, v$, where Δt is the time necessary to reach the next way-point, also defined differential time, Δp is the distance between two consecutive way-points, and v is the cruise velocity. The differential TA at way-point k can be represented by Eq. (10), where $\Delta t_{a,k}$, is the maximum of the three differential TAs computed along x, y, and z direction.

$$\Delta t_{a,k} = \max\left\{\Delta t_{a,x_k}, \Delta t_{a,y_k}, \Delta t_{a,z_k}\right\} \quad , \tag{10}$$

Based on the assumption of normal distribution of the cruise velocity, the uncertainty in the differential TA, can be computed according to error intervals [17] as denoted in Eqs. (11)- (12).

$$\sigma^2_{t_{j,k}} \triangleq \begin{cases} {\Delta t_{a,k}}^2 \, \frac{\sigma^2_{v_{j,k}}}{\bar{v}^2_{j,k}} & \forall \quad \bar{v}_{j,k} \in \bar{\boldsymbol{v}}_k : \bar{v}_{j,k} \neq 0 \\ 0 & \text{otherwise} \end{cases} \tag{11}$$

$$\sigma^2_{t_k} \triangleq \max_{j\in\{x,y,z\}} \left\{\sigma^2_{t_{j,k}}\right\} \tag{12}$$

The variance of the TA at every way-point is equal to the cumulative sum of variances $\sigma^2_{t_i}, \forall\, i \leq k$.

$$\sigma^2_{t_{a,k}} = \sum_{i=1}^{k} \sigma^2_{t_i} \quad . \tag{13}$$

Once Eqs. (11), (12) and (13) are applied to all way-points, the flight plan information is intrinsically enhanced by a Gaussian probability density function (pdf) describing the TA at all way-points:

$$t_{a,k} \sim \mathcal{N}\left(\bar{t}_{a,k}, \sigma^2_{t_{a,k}}\right) \quad , \tag{14}$$

where $\bar{t}_{a,k}$ is the expected value of the time of arrival, or ETA, at way-point k.

The methodology can be easily adjusted to deal with airspeed and wind speed uncertainty, under the assumption of stationary wind field, i.e, when $\partial w(x, y, z, t)/\partial t \approx 0$. In that case, the variance affecting wind speed adds to the variance of the cruise airspeed, owing to the relationship between airspeed, ground speed, and wind speed, $\boldsymbol{v}_g = \boldsymbol{v}_a + \boldsymbol{w}$. The hypothesis of stationary wind profile may be valid for short flights (typical of small UAV for, e.g., delivery of goods), but cannot be directly applied to longer flights where the wind field cannot be considered as stationary.

Once the probability distributions of TAs at every way-point are calculated, the computation of the uncertainty bounds for the entire trajectory is carried out by using the NURBS algorithm three times. First the expected, i.e., "average" trajectory, computed with the ETAs, and then two trajectories

computed using the upper and lower bounds of the TAs, as in Eq. (15), as depicted in Figures 4.

$$\begin{aligned}\boldsymbol{\mathcal{P}}^{+}(t) &= \text{NURBS}(\boldsymbol{P}, \boldsymbol{t}_a^{+}) \\ \boldsymbol{\mathcal{P}}^{-}(t) &= \text{NURBS}(\boldsymbol{P}, \boldsymbol{t}_a^{-})\end{aligned} \tag{15}$$

The TA vectors $\boldsymbol{t}_a^{+}, \boldsymbol{t}_a^{-}$ are defined as follows,

$$\boldsymbol{t}_a^{+} = [\bar{t}_{a,0}, \bar{t}_{a,1} + \sigma_{t_a,1}, \ldots, \bar{t}_{a,K} + \sigma_{t_a,K}] \quad ,$$

$$\boldsymbol{t}_a^{-} = [\bar{t}_{a,0}, \bar{t}_{a,1} - \sigma_{t_a,1}, \ldots, \bar{t}_{a,K} - \sigma_{t_a,K}] \quad .$$

The matrix $\boldsymbol{P} \in \mathbb{R}^{\mathrm{K}\times 3}$ collects the K way-points in x, y, and z directions column-wise, and NURBS$(\cdot)$ has been used to define the NURBS algorithm, which returns the 4D trajectory profile, with corresponding time derivatives, from the input way-points $\boldsymbol{P}$ and TAs $\boldsymbol{t}_a$. The resulting profile is $\boldsymbol{\mathcal{P}}(t)$, which contains the entire trajectory kinematic profile, and where the superscript $+$ and $-$ indicate the upper and lower intervals.

Variance in the cruise velocity introduces uncertainty in the time that the UAV takes to fly from one way-point to the other. Such uncertainties at every position introduces cumulative delay throughout the flight, which is further increased when ETA is computed for the later way-points. Hence as observed from the Figures 4 (a) , the uncertainty bounds are higher towards the end of the trajectory than at the beginning.

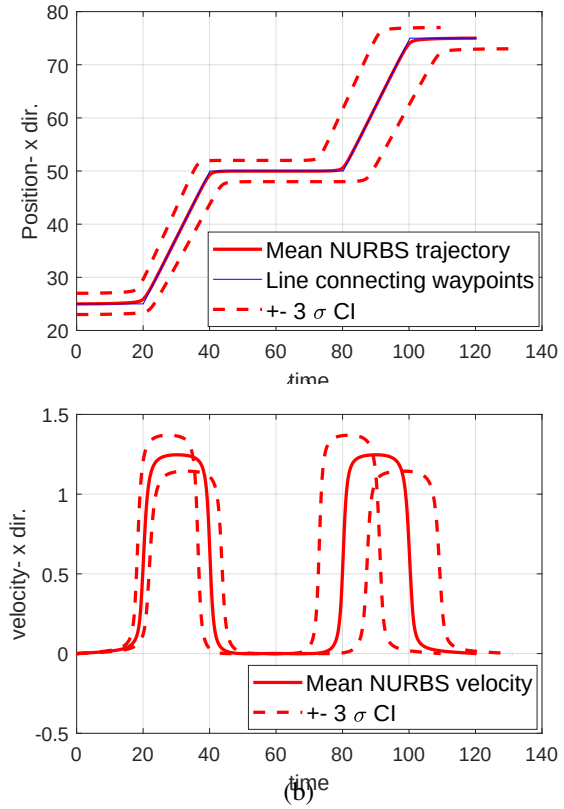

Figure 4. Simulated NURBS trajectory with uncertainty bounds due to variance in cruise velocity (a) position profile and (b)velocity profiles.

Trajectory Estimation using Kalman Filtering

Next, the trajectory profile is converted to a discrete time-state space model and Bayes filtering is implemented to adjust the mean and variance of the UAV position based on the on-board navigation measurements and their covariance matrices. The procedure for computing position estimates along x-direction from NURBS trajectory by incorporating quality of in-time measurements are described in the following steps. The same method is extended to generate position estimates along the other directions.

1. *Initialization*: The NURBS trajectory defined in Eq. (7), together with the uncertainty on the time of arrival from Eq. (14), define the prior PDF of the position estimates at time $t = 0$ s and velocity estimates at time $t = 0$ and $t = 1$ s. The standard deviation for each of the prior PDFs are obtained from the uncertainty bounds computed acording to Eqs. (15), such as

$$\begin{aligned}\sigma_{d,t=t_0} = \max(&\boldsymbol{\mathcal{P}}^{+}(t=t_0) - \boldsymbol{\mathcal{P}}(t=t_0), \\ &\boldsymbol{\mathcal{P}}^{-}(t=t_0) - \boldsymbol{\mathcal{P}}(t=t_0)) \quad ,\end{aligned}$$

while priors of position and velocity are defined as in Eq. (18).

$$d_0^p \sim \mathcal{N}\left(P_{t=t_0}, \sigma^2_{d,t=t_0}\right) \tag{16}$$

$$v_0^p \sim \mathcal{N}\left(V_{t=t_0}, \sigma^2_{v,t=t_0}\right) \tag{17}$$

$$v_1^p \sim \mathcal{N}\left(V_{t=t_1}, \sigma^2_{v,t=t_1}\right) \tag{18}$$

2. *Model Prediction*: In order to generate the state-space model for trajectory update, uniform acceleration profile is assumed for time interval in between two time-stamps or in between two consecutive measurements.If navigation measurements are received from the UAV at frequency of 1 Hz, the position PDF d_1 at the next time-stamp can be computed according to the laws of uniformly accelerated motion, as stated in Eq. (20).

$$d_t = d_{t-1}^p + v_{t-1}^p \delta t + \frac{1}{2} a_{t-1} t\, \delta t^2 \tag{19}$$

$$= d_{t-1}^p + v_{t-1}^p t + \frac{1}{2}(v_t^p - v_{t-1}^p)\delta t \tag{20}$$

Hence, the position can be interpreted as a function of position at the previous time step and parameters $\boldsymbol{\theta}_{t-1:t} = (v_{t-1}, v_t^p)$. It should be noted that in this work, unlike typical state-space models defined in previous works [18], the state at a time step, depends not only on the previous time states but also on parameters at the current time step which are pre-computed from the NURBS trajectory. The velocity value v_t^p obtained from the NURBS velocity profile is a necessary input to the model, since this is the parameter that drives the estimated trajectory towards the planned path dictated by the way-points. In previous works [18], the position of a moving object at a current time step is computed by adding the product of velocity and time interval to the position computed at previous time-step, under the assumption of constant velocity for the entire flight. This is particularly not valid for short UAV flights, since the velocity with which an autonomous UAV flies depends on several factors such as distance between two way-points, wind velocity, obstacle proximities and other mission objectives. For such cases, assuming constant velocity profile for entire UAV operations may yield inaccurate estimation and prediction of the future trajectory.

The implementation of the model follows a Kalman filter formulation as in Eq. (21), which can also be retrieved from many Engineering text books [19]. The terms in Eq. (21) are: the state vector $\boldsymbol{x} = [d_x, d_y, d_z, v_x, v_y, v_z]^T$, containing the three positions d and velocities v in the three Cartesian directions. The input vector containing the planned velocity at the next time step, $\boldsymbol{u}_{k-1} = [v^p_{x,k}, v^p_{y,k}, v^p_{z,k}]^T$. A position error term $\boldsymbol{e}$ used to correct any bias that may be introduced by initial conditions or external disturbances, $\boldsymbol{e}_{k-1} = [e_{x,k-1}, e_{y,k-1}, e_{z,k-1}]^T$. The latter can be seen as control term proportional to the error between planned and observed position.

$$\begin{aligned} \hat{\boldsymbol{x}}_{k|k-1} &= A\,\hat{\boldsymbol{x}}_{k-1|k-1} + B\,\boldsymbol{u}_{k-1} + E\,\boldsymbol{e}_{k-1} \\ P_{k|k-1} &= A\,P_{k-1|k-1}\,A^T + Q \end{aligned} \tag{21}$$

In this formulation, the state matrix A, input matrix B, and error-correction matrix E become:

$$A = 0.5 \begin{bmatrix} 0_3 & I_3 \\ 0_3 & 0_3 \end{bmatrix}$$

$$B = 0.5 \begin{bmatrix} I_3 \\ 0_3 \end{bmatrix}$$

$$E = k_p \begin{bmatrix} I_3 \\ 0_3 \end{bmatrix}$$

where k_p is a constant analogous to the proportional control gain, while 0_3 and I_3 are an all-zero matrix and the identity matrix, both of dimensions 3×3. The constant 0.5 in matrices A and B comes from the approximation of uniformly-accelerated motion where acceleration is computed as the average between speed at two subsequent time steps (see Eq. (20)). Matrices P and Q are the convariance matrix of the state vector P, and the model noise covariance matrix Q. Their dimension is 6×6, following the system state vector. They are both diagonal matrices where each diagonal element represents the variance of the model error in that particular dimension. As obvious from Eq. (21), the filter needs the initialization of both system state vector $\boldsymbol{x}_{k-1|k-1}$ and covariance matrix $P_{k-1|k-1}$.

3. *Updating*: Once the prior of the system state $\hat{\boldsymbol{x}}_{k|k-1}$ and its covariance matrix $P_{k|k-1}$ have been computed, the updating is performed following the Kalman filter procedure, Eq. (22).

$$\begin{aligned} \tilde{\boldsymbol{y}}_k &= \boldsymbol{m}_k - H\,\hat{\boldsymbol{x}}_{k|k-1} \\ S_k &= H\,P_{k|k-1}\,H^T + \Sigma_{meas} \\ K_k &= P_{k|k-1}\,H^T\,S_k^{-1} \\ \hat{\boldsymbol{x}}_{k|k} &= \hat{\boldsymbol{x}}_{k|k-1} + K_k\,\tilde{\boldsymbol{y}}_k \\ P_{k|k} &= (I - K_k\,H)\,P_{k|k-1} \end{aligned} \tag{22}$$

The three position measurements are collected in vector $\boldsymbol{m}$. Matrix H represents the measurement model, while Σ_{meas} represents the covariance of the measures. Matrix K represents the Kalman gain, and the last two rows of Eq. (22) are the posterior estimates of state and covariance matrix. It should be noticed that when both position and velocity are observed, the dimension of all matrices should change accordingly.

Trajectory Prediction

After computing the posterior estimate of the system state, composed of state vector $\hat{\boldsymbol{x}}_{k|k}$ and covariance matrix $P_{k|k}$, the prediction of the remaining trajectory involves the propagation of the state vector through the model, which corresponds to the prediction step of Kalman filtering, Eq. (21). It is a step-by-step simulation of the model following the desired trajectory represented by the NURBS velocity values $v_{.,k}$ in the input vector $\boldsymbol{u}$, and the error-correction term $E\,\boldsymbol{e}$.

On the other hand, the propagation of uncertainty through the covariance matrix $P_{k|k}$ cannot directly follow Eq. (21). If $P_{k|k-1}$ is computed with Eq. (21) over a number of time steps, the covariance terms increase indiscriminately, thus producing large variance values not representative of the real uncertainty. The reason is that the effect of the UAV controller, which keeps the vehicle close to the pre-defined track, is not accounted for when using the second row of Eq. (21).

At this stage of the work, the posterior covariance obtained from $P_{k|k}$ is kept constant throughout the remaining path the UAV has to execute. In this way, the confidence intervals of the UAV location remain constant when the UAV is moving at constant speed, while they increase when there's a change in direction, which implies a change in the velocity vector, as shown in Section 4. where the approach is applied to experimental flight data.

4. Results on Real Data from UAV Flight Experiments

The proposed method of trajectory generation using in-time position measurements is demonstrated on an experimental flight executed by a *DJI S1000* octocopter at NASA Langley Research Center, as shown in Figure 5 (a). The vehicle was equipped with Pixhawk autopilot hardware (`http://pixhawk.org/`) and commanded with Ardupilot software (`http://ardupilot.org/`).

Figure 5 (b) represents the flight plan consisting of a series of 17 waypoints with total flight time of approximately 380 seconds. The measured position of the UAV during flight, which was estimated from on-board navigation units, are plotted in the same Figures. These measured values were utilized in a playback mode to validate the proposed state-space model and compare the predicted position profile with uncertainty bounds against experimental observations. In this experiment, the measurements used by the Pixhawk controller comprised of a filtered estimate of the two navigation devices in the UAV: the global position system (GPS) that uses satellite information and the on-board inertial measurement unit (IMU) which computes the vehicle's acceleration [20]. Thus, the kinematic measurements that ground station receives is a filtered estimate of GPS location with IMU measurements in which the covariance of the filtered estimate is representative of the measurement noise. An example of data quality in terms of covariance of estimated position is available in the MAVLink data under: $Global\_POS\_INT\_COV$ (`https://mavlink.io/en/messages/common.html`).

At first, the position and velocity profile along the latitude dimension is generated using the NURBS algorithm, as depicted by the solid line plots in Figures 6 (a) and(b) respectively. It can be observed Figure 6 (b) that the UAV followed a constant velocity in between the waypoints,

(a)

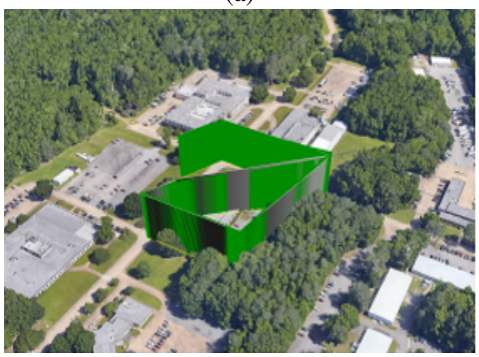

(b)

Figure 5. (a) *DJI S1000* octocopter used for flight tests (Map of flight plan at NASA LARC.

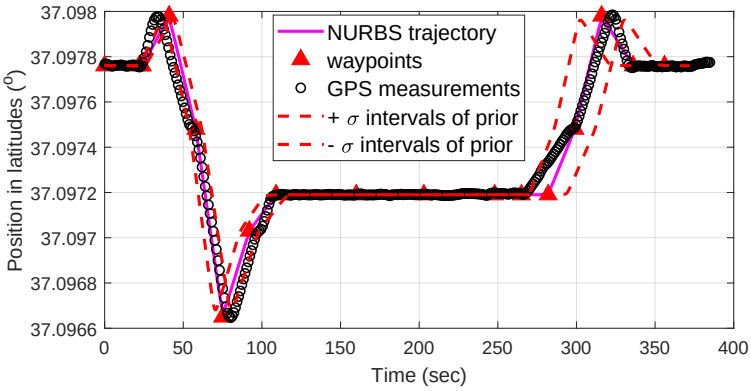

(a)

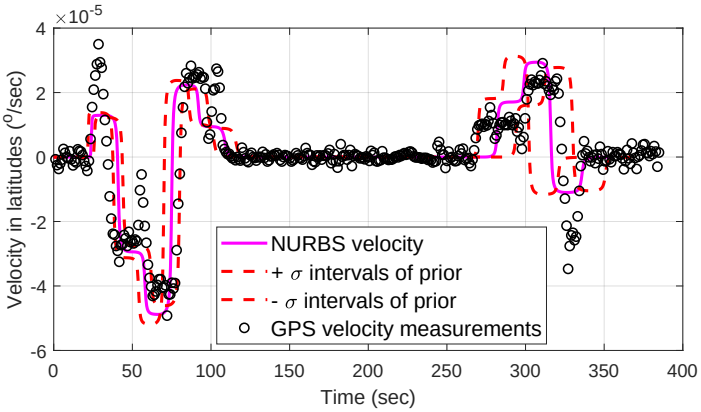

(b)

Figure 6. (a) *DJI S1000* octocopter used for flight tests (b) Map of flight plan at NASA LARC.

yet maintaining a smoother transition as it takes a turn at the waypoint locations. Such kinematic smoothness was achieved by the NURBS simluation. Further, uncertainty was added to the cruise velocity in the form of a normal distribution. A flight executed from the same vehicle, on another day and on another route, was utilized to compute the variance Σ_v of the cruise velocity distribution: $\Sigma_v \approx I_3\,[0.0625, 0.0625, 0.0289]^T$ (m/s)^2. Uncertainty in cruise velocity was then propagated to generate variance in ETA, thereby providing confidence bounds along the entire position and velocity profile as shown by the dashed lines in Figure 6.

The NURBS trajectory along with the confidence bounds represents the prior PDF of the UAV position at time stamp $t = 0$ s. After every interval of 1 second, the measurement along with the covariance of its filtered estimate is utilized to compute the posterior PDF according to Eqs. (21). Additionally, the remaining trajectory is generated following the state-space model using Eq. (22). Figure 7 depicts the estimated and predicted position values along with 95% confidence intervals based on measurements available up to (a) 50, (b) 150 and (c) 280 seconds.

From the three plots it is observed that the proposed method of generating NURBS trajectory followed by the filtering of the state-space model using Kalman filter provided reasonably accurate prediction of future position profile. The measured locations lied within the 95% confidence intervals for most of the trajectory. It can be observed that when measured position lied close to the expected trajectory, the estimated position values were associated with tighter bounds, such as in between $100 - 200sec$ in Figure 7 (c). On the other hand, the velocity is more uncertain at the transition spots when the UAV changes its direction. As a result, the confidence bounds are higher close to those waypoint locations. Besides, as more measurements were available with increasing time, the uncertainty bounds became tighter representing higher confidence associated with the prediction results.

For certain sections of the trajectory, the UAV deviated substantially from its planned route due to unforeseen reasons, such as detour caused by unplanned geofencing during $260 - 300$ second. Under such circumstances, the dynamic replan strategy, explained in [16], shall be triggered which would regenerate a new prior PDF computed by the NURBS algorithm. Subsequently, the estimated and predicted trajectory by the Bayes filters would be able to take such discrepancies into account, thereby refining the UAV monitoring. The dynamic replan approach falls outside the scope of this paper and hence not been illustrated in these results.

Remarks on the uncertainty affecting trajectory predictions

The research presented in this paper raises a question regarding prediction of future states in an autonomous system with an in-built controller. Typically, when Bayes filters are implemented in prognostic of unconstrained phenomena, it is known that confidence intervals associated with the later stages of prediction increase. This can be explained intuitively, since predictions based on early observations are

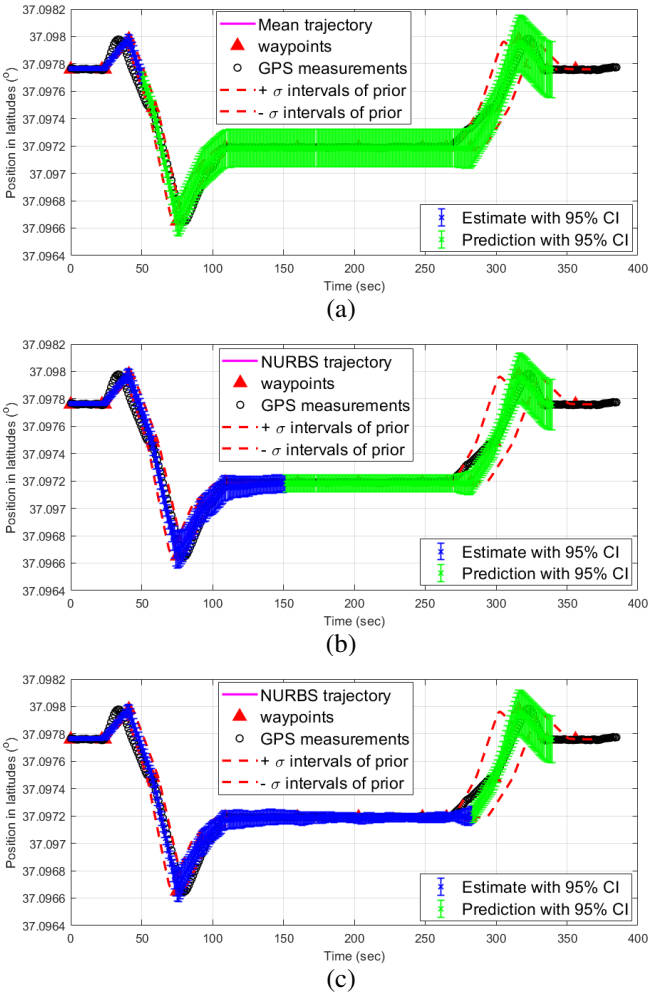

Figure 7. Trajectory estimation and prediction using Bayes filtering with on-board navigation measurements available upto (a) 50 sec (b) 150 sec and (c) 280 sec.

associated with higher uncertainty levels. However, the presence of a controller in ensures that the vehicle is kept close to its pre-defined path. Hence, it is not realistic to increase future prediction uncertainties in an unbounded way. Such controller effect is not accounted for in Kalman filters described in second row of Eq. (21). Hence, implementing Bayes filters in their traditional form may not yield realistic confidence intervals for future trajectory in autonomous UAVs. A possible solution is the use of sampling-based Monte Carlo methods using a medium / high fidelity model to compute exact confidence bounds on the trajectory, for example using particle filtering with a physics-based model with multiple degrees of freedom. However, this may be computationally prohibitive. Simplified ways to propagate uncertainty of predictions of controlled variables is presently under study.

5. Conclusion

This paper presents a comprehensive trajectory tracking approach for an autonomous UAV operation. The methodology leverages existing B-spline algorithm to generate kinematic smooth trajectories which is independent of the vehicle properties. Further, error interval method is implemented to quantify uncertainty in UAV's cruise velocity and propagate to times of arrival at each waypoint, thus generating confidence intervals along the entire NURBS trajectory. The mean position along with the confidence intervals are further refined with available measurements from on-board navigation units using Kalman filters. Unlike previous works, the Kalman filter is adopted on a state-space model which takes both previous and current states as inputs. The proposed modification enables a robust approach to be applicable on a broad category of UAV flights, without enforcing the assumption of constant velocity throughout the entire trajectory. Further, the estimated and predicted trajectory is dependent on the discrepancy in between measured and expected position values as well as on quality of the on-board filtered estimates. Although the results in this paper illustrates a constant variance of measured position, the framework remains valid for varying measurement variances at every time-step.

The above method does not incorporate any vehicle model. Although a control term proportional to the error between planned and observed position is introduced in the model prediction, the simulated path may still not align with an real UAV flight operated by Ardu-pilot software. Particularly, in this paper, only linear dynamics of the vehicle has been studied. Estimates of yaw, pitch, roll and angular velocities require vehicle models which will be incorporated in future work. Safety metrics based on the predicted trajectory such as future power consumption profile, proximity to obstacles or wind effects in urban canyon will be included in the future extensions of this work.

Acknowledgments

This work was supported by the System-Wide Safety (SWS) project under the Airspace Operations and Safety Program within the NASA Aeronautics Research Mission Directorate (ARMD). The authors thank Dr. Andrew Moore and Dr. Patrick Quach from the Dynamic Systems and Control Branch and the Safety Critical Avionics Branch at NASA Langley Research Center, for the flight data utilized in this paper.

References

[1] P. Kopardekar, J. Rios, T. Prevot, M. Johnson, J. Jung, and J. E. Robinson, "Unmanned aircraft system traffic management (utm) concept of operations," in *AIAA Aviation Forum*. AIAA, 2016.

[2] FAA, "Unmanned aerial system (uas) traffic management (utm), concept of operations," Federal Aviation Administration, Tech. Rep., 2018.

[3] S. Henely, "Traffic alert and collision avoidance system ii (tcas ii)," *DIGITAL AVIONICS*, p. 28, 2015.

[4] S. Tsao, "Automated terrain awareness and avoidance system," Mar. 16 2004, uS Patent 6,708,091.

[5] I. Roychoudhury, L. Spirkovska, M. Daigle, E. Balaban, S. Sankararaman, C. Kulkarni, S. Poll, and K. Goebel, "Real-time monitoring and prediction of airspace safety," National Aeronautics and Space Administration, Tech. Rep., 2015.

[6] I. Roychoudhury, L. Spirkovska, M. Daigle, E. Balaban, S. Sankararaman, C. S. Kulkarni, S. Poll, and

K. Goebel, "Predicting real-time safety of the national airspace system," in *AIAA Infotech@ Aerospace*, 2016, p. 2131.

[7] L. Spirkovska, I. Roychoudhury, M. Daigle, and K. Goebel, "Real time safety monitoring: Concept for supporting safe flight operations," in *17th AIAA Aviation Technology, Integration, and Operations Conference*, 2017, p. 4494.

[8] S. D. Young, C. P. Quach, K. Goebel, and J. Nowinski, "In-time safety assurance systems for emerging autonomous flight operations," in *2018 IEEE/AIAA 37th Digital Avionics Systems Conference (DASC)*. IEEE, 2018, pp. 1–10.

[9] "Aeronautics research mission directorate strategic implementation plan , author=National Aeronautics and Space Administration, journal=[Online] https://www.nasa.gov/aeroresearch/strategy, year=Mar 23, 2017."

[10] I. Roychoudhury, L. Spirkovska, M. Daigle, E. Balaban, S. Sankararaman, C. Kulkarni, S. Poll, and K. Goebel, "Real-time monitoring and prediction of airspace safety," 2018.

[11] M. Daigle and C. S. Kulkarni, "End-of-discharge and end-of-life prediction in lithium-ion batteries with electrochemistry-based aging models," in *AIAA Infotech@ Aerospace*, 2016, p. 2132.

[12] E. Ancel, F. M. Capristan, J. V. Foster, and R. C. Condotta, "In-time non-participant casualty risk assessment to support onboard decision making for autonomous unmanned aircraft," in *AIAA Aviation 2019 Forum*, 2019, p. 3053.

[13] M.-Y. Cheng and Y.-H. Wang, "Velocity field construction for contour following tasks represented in nurbs form," *IEEE Transactions on Automatic Control*, vol. 54, no. 10, pp. 2405–2410, 2009.

[14] Y. Bouktir, M. Haddad, and T. Chettibi, "Trajectory planning for a quadrotor helicopter," in *2008 16th mediterranean conference on control and automation*. Ieee, 2008, pp. 1258–1263.

[15] D. F. Rogers, *An introduction to NURBS: with historical perspective*. Elsevier, 2000.

[16] M. Corbetta, P. Banerjee, W. Okolo, G. Gorospe, and D. Luchinsky, "Real-time uav trajectory prediction for safety monitoring in low-altitude airspace," in *AIAA Aviation Forum, UAS Traffic Management IV Session*. AIAA, 2019.

[17] O. Miller, "A summary of error propagation," 2013, harvard University, Physical Sciences 2, Lecture Notes.

[18] Q.-L. Zhou, Y. Zhang, Y.-H. Qu, and C.-A. Rabbath, "Dead reckoning and kalman filter design for trajectory tracking of a quadrotor uav," in *Proceedings of 2010 IEEE/ASME International Conference on Mechatronic and Embedded Systems and Applications*. IEEE, 2010, pp. 119–124.

[19] R. E. Kalman, "A new approach to linear filtering and prediction problems," *Journal of basic Engineering*, vol. 82, no. 1, pp. 35–45, 1960.

[20] L. Meier, P. Tanskanen, F. Fraundorfer, and M. Pollefeys, "Pixhawk: A system for autonomous flight using onboard computer vision," in *2011 IEEE International Conference on Robotics and Automation*. IEEE, 2011, pp. 2992–2997.

BIOGRAPHY

Portia Banerjee *received her Bachelors of Technology degree in Electronics and Communications Engineering from National Institute of Technology Durgapur, India and her Ph.D. in Electrical and Computer Engineering from Michigan State University. Being an author of several journals and conference papers, she is currently working on health monitoring of unmanned aviation systems as a research engineer with SGT Inc. at NASA Ames Research Center, CA. Her research interests include statistical signal processing, image processing, data mining, uncertainty management and reliability analysis focusing towards diagnostic and prognostic applications in structures and autonomous systems. She is a member of the AIAA, IEEE and ASME societies and is a member of the Executive Committee of ASME NDE Diagnosis and Prognosis Division.*

Matteo Corbetta *is a Research Engineer with SGT Inc. at NASA Ames Research Center, CA, where he is investigating uncertainty quantification methods, model-based and data-driven algorithms for diagnostics and prognostics of engineering systems, particularly autonomous vehicles. Prior to joining NASA, he worked as R&D Condition Monitoring Systems Engineer at Siemens Wind Power, Denmark, and as Post-Doctoral Researcher and Teaching Assistant at Politecnico di Milano, Italy, where he received Ph.D., MSc. and BSc. in Mechanical Engineering. His research interests include stochastic processes, algorithms for uncertainty quantification, machine learning, and system health management. He is member of AIAA, IEEE, and member of the Editorial Board of the PHM Society.*